Out-of-plane heat transfer in van der Waals stacks through electron-hyperbolic phonon coupling

Klaas-Jan Tielrooij,[1,*] Niels C. H. Hesp,[1] Alessandro Principi,[2] Mark B. Lundeberg,[1] Eva A. A. Pogna,[3] Luca Banszerus,[4] Zoltán Mics,[5] Mathieu Massicotte,[1] Peter Schmidt,[1] Diana Davydovskaya,[1] David G. Purdie,[6] Ilya Goykhman,[6] Giancarlo Soavi,[6] Antonio Lombardo,[6] Kenji Watanabe,[7] Takashi Taniguchi,[7] Mischa Bonn,[5] Dmitry Turchinovich,[5] Christoph Stampfer,[4] Andrea C. Ferrari,[6] Giulio Cerullo,[3] Marco Polini,[8] and Frank H. L. Koppens[1,9,*]

[1]*ICFO - Institut de Ciències Fotòniques, The Barcelona Institute of Science and Technology, Castelldefels (Barcelona) 08860, Spain*

[2]*Radboud University, Institute for Molecules and Materials, NL-6525 AJ Nijmegen, the Netherlands*

[3]*IFN-CNR, Dipartimento di Fisica, Politecnico di Milano, Piazza L. da Vinci 32, 20133 Milano, Italy*

[4]*JARA-FIT and 2nd Institute of Physics, RWTH Aachen University, 52074 Aachen, Germany*

[5]*Max Planck Institute for Polymer Research, Ackermannweg 10, Mainz 55128, Germany*

[6]*Cambridge Graphene Centre, University of Cambridge, Cambridge CB3 OFA, UK*

[7]*National Institute for Material Science, 1-1 Namiki, Tsukuba 305-0044, Japan*

[8]*Istituto Italiano di Tecnologia, Graphene Labs, Via Morego 30, I-16163 Genova, Italy*

[9]*ICREA - Institució Catalana de Reçerca i Estudis Avancats, 08010 Barcelona, Spain*

Abstract

Van der Waals heterostructures have emerged as promising building blocks that offer access to new physics, novel device functionalities, and superior electrical and optoelectronic properties[1–7]. Applications such as thermal management, photodetection, light emission, data communication, high-speed electronics and light harvesting[8–16] require a thorough understanding of (nanoscale) heat flow. Here, using time-resolved photocurrent measurements we identify an efficient out-of-plane energy transfer channel, where charge carriers in graphene couple to hyperbolic phonon polaritons[17–19] in the encapsulating layered material. This hyperbolic cooling is particularly efficient, giving picosecond cooling times, for hexagonal BN, where the high-momentum hyperbolic phonon polaritons enable efficient near-field energy transfer. We study this heat transfer mechanism through distinct control knobs, such as carrier density and lattice temperature, and find excellent agreement with theory without any adjustable parameters. These insights may lead to the ability to control heat flow in van der Waals heterostructures.

*Electronic address: Correspondence:klaas-jan.tielrooij@icfo.eu,frank.koppens@icfo.eu

Owing to its large in-plane thermal conductivity, graphene has been suggested as material for the thermal management of nanoscale devices[8]. At the same time, graphene is well-known for its ability to convert incident light into electrical heat, i.e. hot electrons that can be used to generate photocurrent, with applications in photodetection, data communication and light harvesting[10, 20, 21]. Understanding, and ultimately controlling, heat flow in graphene-van der Waals heterostructures is therefore of paramount importance. E.g., a short cooling time of graphene hot carriers is advantageous for thermal management and for high switching rates of photodetectors (PDs) for data communication, whereas a long cooling time is favorable for photodetection sensitivity[10, 20, 21]. Of particular relevance are heterostructure devices that contain high-quality graphene encapsulated by layered materials, such as hexagonal BN (hBN) and MoS_2, which have the potential to crucially improve the performance of electronic and optoelectronic devices[1, 2].

A number of cooling pathways for graphene carriers have been proposed, involving among others strongly coupled optical phonons[22–24], acoustic phonons[25–28], substrate phonons[29] and plasmons[30] (see also Supp. Section 1). Here, using several experimental approaches, we show that cooling in graphene encapsulated by hBN is governed by out-of-plane coupling of graphene electrons to special polar phonon modes that occur in layered materials (LMs): hyperbolic phonon polaritons, where $\epsilon_{xx}\epsilon_{zz} < 0$, with ϵ_{xx} and ϵ_{zz} the permittivity parallel and perpendicular to the LM plane. Owing to this property, these materials carry deep sub-wavelength, ray-like optical phonon polaritons. For hBN, within the two Reststrahlen bands a large number of hyperbolic phonon modes exist with high momenta, far outside the light cone. The most notable modes occur at an energy of $\sim$100meV and $\sim$180meV[17], such that energy overlap with the graphene hot-carrier distribution is substantial. The unusual hyperbolic character gives rise to a very high density of optical states, and thus large thermal energy densities[17, 18], thereby providing a potentially efficient cooling pathway for hot carriers in graphene. By near-field coupling between graphene and hBN, efficient energy transfer from hot carriers to hyperbolic phonon polaritons is possible[31]. Here we show that the measured carrier dynamics of hBN-encapsulated graphene can be explained by this hyperbolic cooling process, as illustrated in Fig. 1a.

We use ultrafast time-resolved photocurrent measurements and show the results obtained from one hBN-encapsulated, Hall-bar shaped, exfoliated graphene device (see Fig. 1b). The device contains chemical vapor deposited (CVD) graphene split gates underneath the bottom hBN (thickness: 70 nm), in order to generate a *pn*-junction in the middle of the device. A second hBN-encapsulated device with metallic split gates gave fully consistent results. With 800nm light incident on the *pn*-junction, a photovoltage is generated by the photo-thermoelectric (PTE) effect[20, 21] (see the photocurrent and reflection data in Supp. Fig. 1 and the characteristic PTE sixfold pattern in Supp. Fig. 2). By varying the delay Δt between two sub-picosecond pulses we extract the carrier dynamics from the photovoltage signal $\Delta V_{\mathrm{PTE}}(\Delta t)$ (see Fig. 1c). Since the photo-thermoelectric voltage scales with the light-induced increase in carrier temperature, the decay dynamics of $\Delta V_{\mathrm{PTE}}(\Delta t)$ closely mimic the cooling dynamics of the hot electron system (see Supp. Fig. 3 for an analysis of the extent to which the experimentally observed decay dynamics correspond to the underlying cooling dynamics). In the case of exponential decay dynamics, which we observe above a lattice temperature of ∼200 K, we extract an experimental cooling time scale τ_{exp} by describing the decay dynamics with $\Delta V_{\mathrm{PTE}}(\Delta t) \propto e^{-\Delta t/\tau_{\mathrm{exp}}}$.

First, we electrically characterize our device using four-probe measurements (see Fig. 2a) and find a mean free path of $k_{\mathrm{F}}\ell = 80$–100 at a carrier density of $n = 1.7 \times 10^{12}/\mathrm{cm}^2$, corresponding to a mobility of 25,000–30,000 $\mathrm{cm}^2/\mathrm{Vs}$ and momentum scattering time of 340–440 fs. As expected, this is much higher than SiO_2-supported devices with typically $k_{\mathrm{F}}\ell < 10$, mobility $< 5{,}000$ $\mathrm{cm}^2/\mathrm{Vs}$ and momentum scattering time < 100 fs (see e.g. Ref. [27]). In such devices, carrier cooling is typically ascribed to disorder-assisted cooling to graphene acoustic phonons [26–28].

To study hot-carrier cooling in our high-mobility, encapsulated devices we examine $\Delta V_{\mathrm{PTE}}(\Delta t)$ while varying graphene's most characteristic parameter, the carrier density n. In particular, we apply a gate voltage $V_{\mathrm{L}} = +V - V_{\mathrm{D}}$ to the left split gate and $V_{\mathrm{R}} = -V - V_{\mathrm{D}}$ to the right gate, such that there is always either a *pn*-junction or an *np*-junction, with equal electron and hole densities in the two graphene regions (V_{D} is the gate voltage that corresponds to the Dirac point). The incident laser fluence is typically 5 – 40 $\mu\mathrm{J}/\mathrm{cm}^2$. The data show that cooling becomes faster upon increasing the carrier density (see Fig.

2b). We also vary the lattice temperature T_{L} and observe faster decay for increasing lattice temperature (see Fig. 2c, taken at $n \approx 10^{12}/\mathrm{cm}^2$). At low temperatures (below $\sim$200 K), cooling is non-exponential, whereas at room temperature we observe exponential decay of the photovoltage dip, with a timescale of $\tau_{\mathrm{exp}} \approx 2.5$ ps (for $n = 1.7 \times 10^{12}/\mathrm{cm}^2$). We independently verify this cooling time using two alternative measurement techniques that are both sensitive to electron cooling dynamics in different ways (see Supp. Fig. 4). Firstly, using ultrafast optical pump – optical probe spectroscopy, which probes interband transitions[24], we find τ_{exp}= 2.55 ps for the decay of the absorption photobleaching. Secondly, using optical pump – terahertz probe spectroscopy, which probes intraband transitions [13], we obtain $\tau_{\mathrm{exp}} = 2.2$ ps for the decay of the photoconductivity. For these two experiments we use similar excitation conditions (an incident pulse fluence of 8–20 $\mu\mathrm{J}/\mathrm{cm}^2$) as in the photocurrent measurements, and the measurements are performed on two separate devices consisting of large-area, high-quality hBN-encapsulated CVD graphene as in Ref. [32]. Thus, all three techniques consistently yield similar cooling times for hBN-encapsulated graphene.

We compare these observations with different cooling mechanisms, and note that the data are qualitatively and quantitatively inconsistent with in-plane cooling by scattering with graphene acoustic phonons through normal[25] or disorder-assisted collisions[26–28] (see Supp. Section 1 and Supp. Fig. 5). In-plane cooling can also occur by scattering to graphene optical phonons, typically occurring on a sub-picosecond timescale[22, 24]. Reference[23] reports that for *non-encapsulated* graphene this channel gives picosecond decay dynamics of the THz photoconductivity. However these results deviate in several ways from our observations for hBN-encapsulated graphene (see Supp. Section 1). For example, we observe a twofold increase in cooling time by decreasing T_{L} from 300 K to 200 K, whereas optical phonon cooling gives cooling dynamics that are independent of substrate temperature (for $E_{\mathrm{F}} = 0.3$ eV), see Ref. [23]. This indicates that, besides a fraction of hot graphene electrons possibly cooling through optical phonons, a different cooling mechanism plays an important role. Since we observe a striking effect of the hBN crystal slab thickness on the cooling dynamics (see Supp. Fig. 6 and Supp. Section 2), we propose an out-of-plane cooling mechanism where hot carriers in graphene lose their energy to remote polar phonons in the encapsulating layered material. The energy transfer can be understood from fluctua-

tion electrodynamics, where any process that dissipates energy in the form of heat, has a reverse process that is driven by thermal fluctuations and thus becomes stronger at higher temperatures[33, 34]. An example of such paired processes is light absorption and blackbody radiation, which means that graphene emits thermal noise due to the dissipative real part (indicated by $\mathcal{R}$) of the frequency- and momentum-dependent optical sheet conductivity $\sigma(\omega, k)$. This thermal noise is efficiently absorbed by hBN, hBN being a lossy-polarizable material, leading to an energy transfer rate [31]:

$$\mathcal{Q} = \iiint_{-\infty}^{\infty} \frac{d\omega dk_x dk_y}{(2\pi)^3} [n_B(\omega, T_\mathrm{e}) - n_B(\omega, T_\mathrm{L})] M(\omega, k) \quad , \tag{1}$$

where $n_B(\omega, T) = \frac{\hbar|\omega|}{e^{\hbar|\omega|/k_\mathrm{B}T}-1}$ and $M(\omega, k) = 4\frac{\mathcal{R}\{Y(\omega,k)\}\mathcal{R}\{\sigma(\omega,k)\}}{|Y(\omega,k)+\sigma(\omega,k)|^2}$ (k_B is Boltzmann's constant). Heat transfer from hot graphene electrons to hBN hyperbolic phonon polaritons is thus governed by the Bose factor $[n_B(\omega, T_\mathrm{e}) - n_B(\omega, T_\mathrm{L})]$, which describes the energy disequilibrium between hot graphene carriers and the cold hBN phonon system, and the impedance matching function $M(\omega, k)$, which is nonzero when the surface admittance $Y(\omega, k)$ has a nonzero real part. We calculate $Y(\omega, k)$ as in Ref. [35] (see Methods for details) and find that nearby the hyperbolic hBN phonon frequencies $Y(\omega, k)$ is real over a large k-space area and relatively wide frequency band. Since $\sigma(\omega, k)$, calculated using the Random Phase Approximation[36], also has a significant real part, this leads to an impedance matching function M approaching unity. Due to this near-field coupling to hyperbolic modes, the heat conductivity exceeds Planck's law for blackbody radiation by orders of magnitude (see Supp. Fig. 7). The reason for this is that in vacuum, the k-space for blackbody radiation is limited to $k < \omega/c$ (with c the speed of light), whereas this restriction is lifted in the near-field interaction with hBN hyperbolic phonon polaritons. This super-Planckian coupling to hyperbolic hBN phonons thus provides a highly efficient cooling channel for hot carriers in graphene. Cooling to hyperbolic modes also occurs in materials such as MoS_2, although there it is not as efficient as for hBN (see Supp. Fig. 7).

To compare our hyperbolic cooling theory with the experimental data, we examine the calculated energy transfer rate $\mathcal{Q}$. Here, solving Eq. (1) gives cooling dynamics with a cooling time scale

$$\tau_\mathrm{calc}(T_\mathrm{e}, T_\mathrm{L}) = C_\mathrm{n} \frac{T_\mathrm{e} - T_\mathrm{L}}{\mathcal{Q}} \quad , \tag{2}$$

where C_n is the electronic heat capacity of graphene at constant n [31]. In the limit of weak

heating, where T_e approaches T_L, we obtain exponential decay with the near-equilibrium timescale $\tau_{calc}(T_e \rightarrow T_L) = \tau^*_{calc} = C_n\left(\frac{\partial \mathcal{Q}}{\partial T_e}\big|_{T_e=T_L}\right)^{-1}$, where $\frac{\partial \mathcal{Q}}{\partial T_e}\big|_{T_e=T_L}$ is the interfacial heat conductivity Γ. We compare the calculated near-equilibrium cooling time τ^*_{calc} with the measured exponential decay time τ_{exp} (see Fig. 3), although strictly speaking these experimental timescales correspond to the strong heating regime, where $T_e \gg T_L$. The reason for this is that our technique is not sensitive enough at low incident powers, which means that experimentally we cannot directly access the near-equilibrium cooling time τ^*_{calc}. Nevertheless, we find that our hyperbolic hBN cooling model semi-quantitatively reproduces the experimentally observed trends for the entire range of investigated carrier densities (up to $1.6\times10^{12}/\mathrm{cm}^2$) and lattice temperatures (200 – 300 K). In particular, cooling slows down for lower lattice temperatures, which we attribute mainly to the smaller Bose factor in Eq. (1) and thus smaller energy transfer rate $\mathcal{Q}$. The calculations also reproduce the observation of a longer cooling time around the Dirac point. This is the result of the energy transfer rate $\mathcal{Q}$ smoothly decreasing towards zero carrier density, while the electronic heat capacity C_n flattens around the Dirac point towards its neutral graphene value (see Supp. Fig. 7). At higher carrier densities ($n > 10^{12}/\mathrm{cm}^2$) the increasing energy transfer rate is compensated by the increasing heat capacity, leading to a weak dependence of cooling time on carrier density. Cooling to hyperbolic modes was also observed in a noise thermometry study[37]. We further note that the two distinct hyperbolic modes contribute almost equally to the overall cooling time, with the lower-energy mode slightly dominant (see Supp. Fig. 7). This can be attributed to more energy overlap in the Bose factor. We note that the hyperbolic cooling model reproduces the observed slower decay dynamics for encapsulation with very thin hBN flakes (see Supp. Fig. 6). In this case, cooling is slower because overall there is a lower density of hyperbolic modes to couple to.

To make a more quantitative comparison, we take into account that the measurements are typically done in the strong heating regime, where $T_e \gg T_L$. We first measure the cooling dynamics for increasing laser power and estimate the electron temperatures that correspond to each power from the characteristic power-dependent photoresponse (see Supp. Fig. 8 and Methods), thus obtaining the exponential decay time τ_{exp} vs. T_e (see Fig. 4a). In the experimentally accessible regime ($\Delta T_e = T_e - T_L > 200$ K) the τ_{exp} increases with increasing T_e (measured for $n = 1.2 \times 10^{12}/\mathrm{cm}^2$). We compare this with the calculated

cooling time τ_{calc}, which describes the "instantaneous" cooling time at a certain T_{e}, and find quantitative agreement *without any adjustable parameters*. The reason for the increasing cooling time with increasing T_{e} can be seen from Eq. (2) and by noting that $\mathcal{Q}/(T_{\mathrm{e}} - T_{\mathrm{L}})$ scales roughly linearly with $(T_{\mathrm{e}} - T_{\mathrm{L}})$. At the same time, the electronic heat capacity C_n, increases more than linearly with increasing T_{e} for large T_{e}. This leads to a net increase in the cooling time with increasing T_{e}. The agreement between experiment and calculation prompts us to make a more quantitative comparison for varying carrier density n. Figure 4b shows τ_{exp} for three different laser powers (P = 21, 47 and 94 μW), corresponding to three different initial hot electron temperatures (ΔT_{e} = 650, 950 and 1250 K), together with the calculated near-equilibrium cooling time τ^*_{calc}. The comparison between experimental results in the strong heating regime (τ_{exp}) and theoretical results close to equilibrium (τ^*_{calc}) is justified in Fig. 4a, where we show that the cooling time at $T_{\mathrm{e}} \sim 1000$ K is similar to τ^*_{calc}. Again we find agreement between experiment and theory *without any adjustable parameters*.

Finally, we compare the calculated time-domain cooling dynamics in the strong heating regime directly with the measured photocurrent dynamics. The calculated cooling dynamics describe cooling from an initial T_{e} down to T_{L}, as constructed from the electron temperature-dependent cooling time τ_{calc} in Eq. (2). We compare these calculated cooling dynamics directly with the measured photovoltage dynamics $\Delta V_{\mathrm{PTE}}(\Delta t)$ for six different lattice temperatures, at a low carrier density of $n = 0.06 \times 10^{12}/\mathrm{cm}^2$ (see Fig. 4c). Using the initial temperature (at the *pn*-junction) as a fit parameter, we find that the hyperbolic cooling model can describe the experimental data very well. At room temperature, the initial temperature is similar to the one we calculate (see Fig. Supp. 8), whereas we find a lower initial temperature at lower lattice temperatures. This is due to the increased mechanical vibrations of the sample and lateral heat diffusion out of the laser spot at lower T_{L}, which both lead to a larger photocurrent spot size and thus a lower effective initial T_{e} at the *pn*-junction (see Supp. Fig. 9). For a lattice temperature of 50 K, we furthermore see an increasing discrepancy for a delay time >15 ps, which most likely indicates that hBN-phonons alone do not account for the complete cooling dynamics. Similarly, we find that at a higher carrier density of $n = 1.7 \times 10^{12}/\mathrm{cm}^2$ the hyperbolic cooling model starts deviating from the experimental data already for $T_{\mathrm{L}} < 200$ K (see Supp. Fig. 10). Most likely, at sufficiently low lattice temperature and sufficiently high carrier density, cooling

through optical phonons [22, 23] and momentum-conserving cooling to acoustic graphene phonons [25, 38, 39] become the dominant channels.

In summary, we addressed the issue of out-of-plane heat transfer in the device architecture of hBN-encapsulated graphene. Combining experiments with microscopic theoretical calculations, we showed that the dominant cooling channel is the one in which heat transfer from hot carriers to the hBN polar substrate occurs via near-field coupling to hyperbolic phonon modes. This efficient mechanism explains the observation of a lower-than-expected cooling time in clean hBN-encapsulated graphene. We note that the observation of slower cooling for thin hBN encapsulation could have important implications for photodetection applications. In addition, we predict that significantly slower cooling can be achieved using alternative layered dielectrics, such as MoS_2. Furthermore, the near-field coupling we studied in this work between hot graphene carriers and hyperbolic hBN phonons may pave the way to novel approaches in fields such as nanophotonics, ultrahigh resolution microscopy and nanoscale thermal management.

References

[1] Geim, A.K. & Grigorieva, I.V. Van der Waals heterostructures *Nature* **499**, 419-425 (2013)

[2] Dean, C.R. et al. Boron nitride substrates for high-quality graphene electronics. *Nature Nanotech* **5**, 722 (2010)

[3] Mayorov, A.S. et al. Micrometer-scale ballistic transport in encapsulated graphene at room temperature. *Nano Lett.* **11**, 2396 (2011)

[4] Britnell, L et al. Electron tunneling through ultrathin boron nitride crystalline barriers. *Nano Lett.* **12**, 1707 (2012)

[5] Dean, C.R. et al. Hofstadter's butterfly and the fractal quantum Hall effect in moiré superlattices. *Nature* **497**, 598 (2013)

[6] Ferrari, A.C. *et al.*, Science and technology roadmap for graphene, related two-dimensional crystals, and hybrid systems *Nanoscale* **7**, 4598 (2015).

[7] Wang, L. et al. One-Dimensional Electrical Contact to a Two-Dimensional Material. *Science*

342, 614-617 (2013)

[8] Balandin, A.A. et al. Superior Thermal Conductivity of Single-Layer Graphene. *Nano Lett.* **8**, 902–907 (2008)

[9] Britnell, L. et al. Strong Light-Matter Interactions in Heterostructures of Atomically Thin Films. *Science* **340** 1311–1314 (2013)

[10] Koppens, F.H.L. et al. Photodetectors based on graphene, other two-dimensional materials and hybrid systems. *Nature Nanotech.* **9**, 780793 (2014)

[11] Lopez-Sanchez, O. et al. Light Generation and Harvesting in a van der Waals Heterostructure. *ACS Nano* **8**, 3042 (2014)

[12] Bonaccorso, F. et al. Graphene, related two-dimensional crystals, and hybrid systems for energy conversion and storage. *Science* **347**, 1246501 (2015)

[13] Mics, Z et al. Thermodynamic picture of ultrafast charge transport in graphene. *Nature Comm.* **6**, 7655 (2015)

[14] Kim, Y.D. et al. Bright visible light emission from graphene. *Nature Nanotech.* **10**, 676-681 (2015)

[15] Massicotte, M. et al. Picosecond photoresponse in van der Waals heterostructures. *Nature Nanotech.* **11**, 42–46 (2016)

[16] Bonaccorso, F., Sun, Z., Hasan, T., Ferrari, A.C. Graphene photonics and optoelectronics *Nat. Photonics* **4**, 611 (2010).

[17] Caldwell, J.D. et al. Sub-diffractional volume-confined polaritons in the natural hyperbolic material hexagonal boron nitride. *Nature Comm.* **5**, 5221 (2014)

[18] Dai, S. et al. Tunable phonon polaritons in atomically thin van der Waals crystals of boron nitride. *Science* **343** 1125 (2014)

[19] Basov, D.N., Fogler, M.M. & Garcia de Abajo, F.J. Polaritons in van der Waals materials. *Science* **354**, 1992 (2016)

[20] Gabor N.M. et al. Hot Carrier-Assisted Intrinsic Photoresponse in Graphene. *Science* **334**, 648-652 (2011)

[21] Song, J.C.W. et al. Hot Carrier Transport and Photocurrent Response in Graphene. *Nano Lett.* **11**, 4688-4692 (2011)

[22] Kampfrath, T. et al. Strongly coupled optical phonons in the ultrafast dynamics of the electronic energy and current relaxation in graphite. *Phys. Rev. Lett.* **95**, 187403 (2005).

[23] Mihnev, M.T. et al. Microscopic origins of the terahertz carrier relaxation and cooling dynamics in graphene. *Nature Comm.* **7**, 11617 (2016)

[24] D. Brida et al., Ultrafast collinear scattering and carrier multiplication in graphene. *Nature Comm.* **4**, 1987 (2013)

[25] Bistritzer, R. & MacDonald, A. H. Electronic cooling in graphene. *Phys. Rev. Lett.* **102**, 206410 (2009).

[26] Song, J.C.W., Reizer, M.Y. & Levitov, L.S. Disorder-Assisted Electron-Phonon Scattering and Cooling Pathways in Graphene. *Phys. Rev. Lett.* **109**, 106602 (2012).

[27] Graham, M.W., Shi, S.-F., Ralph, D.C., Park, J. & McEuen, P.L. Photocurrent measurements of supercollision cooling in graphene. *Nature Phys.* **9**, 103-108 (2013)

[28] Betz, A.C. et al. supercollision cooling in undoped graphene. *Nature Phys.* **9**, 109-112 (2013)

[29] Low, T. et al. Cooling of photoexcited carriers in graphene by internal and substrate phonons. *Phys. Rev. B* **86**, 045413 (2012)

[30] Hamm, J.M. et al. Nonequilibrium plasmon emission drives ultrafast carrier relaxation dynamics in photoexcited graphene. *Phys. Rev. B* **93**, 041408 (2016)

[31] Principi, A. et al. Super-Planckian electron cooling in a van der Waals stack. *Phys. Rev. Lett.* **118**, 126804 (2017)

[32] Banszerus, L. et al. Ultrahigh-mobility graphene devices from chemical vapor deposition on reusable copper. *Science Adv.* **1**, e1500222 (2015)

[33] Nyquist, H. Thermal Agitation of Electric Charge in Conductors. *Phys. Rev.* **32**, 110113 (1928).

[34] Mihnev, M.T. et al. Electronic cooling via interlayer Coulomb coupling in multilayer epitaxial graphene. *Nature Comm.* **6**, 8105 (2015)

[35] Tomadin, A, et al. Accessing phonon polaritons in hyperbolic crystals by angle-resolved photoemission spectroscopy. *Phys. Rev. Lett.* **115**, 087401 (2015)

[36] Giuliani, G.F. & Vignale G. Quantum Theory of the Electron Liquid (Cambridge University Press, Cambridge, 2005)

[37] Yang, W. et al. Hyperbolic cooling of a graphene on hBN transistor in the Zener-Klein regime. *Arxiv:***1702.02829** (2017)

[38] Ma, Q. et al. Competing Channels for Hot-Electron Cooling in Graphene. *Phys. Rev. Lett.* **112**, 247401 (2014)

[39] Jadidi, M.M. et al. Infrared Nonlinear Photomixing Spectroscopy of Graphene Thermal Relaxation. *Phys. Rev. Lett.* **117**, 257401 (2016)

[40] Hwang, E.J., Rossi, E. & Das Sarma, S. Theory of thermopower in two-dimensional graphene. *Phys. Rev. B.* **80**, 235415 (2009)

[41] Wunsch, B. et al. Dynamical polarization of graphene at finite doping. *New J. Phys.* **8**, 318 (2006)

[42] Hwang, E.H. & Das Sarma, S. Dielectric function, screening, and plasmons in two-dimensional graphene, *Phys. Rev. B* **75**, 205418 (2007)

[43] Principi, A., Polini, M. & Vignale, G. Linear response of doped graphene sheets to vector potentials, *Phys. Rev. B* **80**, 075418 (2009)

[44] Kotov, V.N. et al. Electron-Electron Interactions in Graphene: Current Status and Perspectives, *Rev. Mod. Phys.* **84**, 1067 (2012)

[45] Alonso-González, P. et al. Acoustic terahertz graphene plasmons revealed by photocurrent nanoscopy, *Nature Nanotech.* **2**, 3135 (2017)

Acknowledgments

We thank Andrea Tomadin and Fabien Vialla for valuable discussions. This work was supported by the European Union's Horizon 2020 research and innovation programme under grant agreement No. 696656 Graphene Flagship, Fondazione Istituto Italiano di Tecnologia, the Spanish Ministry of Economy and Competitiveness through the Severo Ochoa Programme for Centres of Excellence in R&D (SEV-2015-0522), Fundacio Cellex Barcelona, the Mineco grants Ramon y Cajal (RYC-2012-12281), Plan Nacional (FIS2013-47161-P), and the Government of Catalonia trough the SGR grant (2014-SGR-1535), the ERC StG CarbonLight (307806), ERC Grant Hetero2D, EPSRC Grants EP/K01711X/1, EP/K017144/1, EP/N010345/1, and EP/L016087/1. K.J.T. acknowledges support through the Mineco Young Investigator Grant (FIS2014-59639-JIN). A.P. acknowledges support from the ERC Advanced Grant 338957 FEMTO/NANO and from the NWO via the Spinoza Prize. M.M. thanks the Natural Sciences and Engineering Research Council of Canada (PGSD3-426325-2012). D.T. acknowledges financial support from European Union Marie Curie Program (Career Integration Grant No. 334324 LIGHTER) and Max Planck Society. K.W. and T.T. acknowledge support from the Elemental Strategy Initiative conducted by the MEXT, Japan and JSPS KAKENHI Grant Numbers JP26248061, JP15K21722 and JP25106006.

Author contributions

K.J.T. and F.H.L.K. conceived the experiment. K.J.T. and N.C.H.H. performed the time-resolved photocurrent experiments and performed the data analysis. A.P., M.P. and M.B.L. developed theory and performed calculations on hyperbolic cooling. E.A.A.P. performed the optical pump – probe spectroscopy measurements. Z.M. and K.J.T. performed the optical pump – THz probe spectroscopy measurements. N.C.H.H., M.B.L., L.B., M.M., P.S., D.D., D.G.P, I.G., G.S., and A.L. fabricated devices. K.W. and T.T. contributed hBN material. M.B., D.T., C.S., A.C.F, G.C., M.P. and F.H.L.K. supervised the work and discussed results. K.J.T., F.H.L.K and M.P. wrote the paper with input from all authors.

Author information

The authors declare no conflict of interests.

Figures and captions

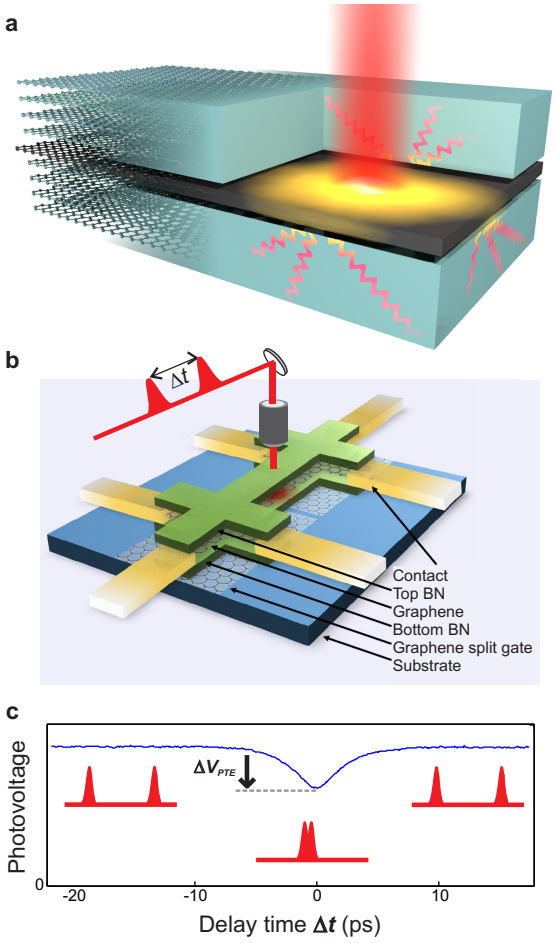

FIG. 1: **Hot carrier cooling in hBN-encapsulated graphene. a)** Schematic representation of out-of-plane heat transfer in hBN-encapsulated graphene: highly efficient near-field emission from graphene hot carriers into directional hyperbolic phonon polaritons of the encapsulating material. **b)** Schematic drawing of the hBN-encapsulated graphene device with graphene split gates. By applying a different voltage to the two split gates we create a *pn*-junction in the encapsulated graphene layer, which we illuminate with two ultrafast pulses that arrive with a variable time delay Δt. **c)** The resultant photo-thermoelectric photovoltage measured between two contacts shows a dip when the two ultrafast pulses overlap. This is due to the nonlinear relation between hot carrier temperature and incident light intensity. The dynamics of the photovoltage dip ΔV_{PTE} as a function of time delay Δt therefore correspond to the cooling dynamics of the hot carriers at the *pn*-junction.

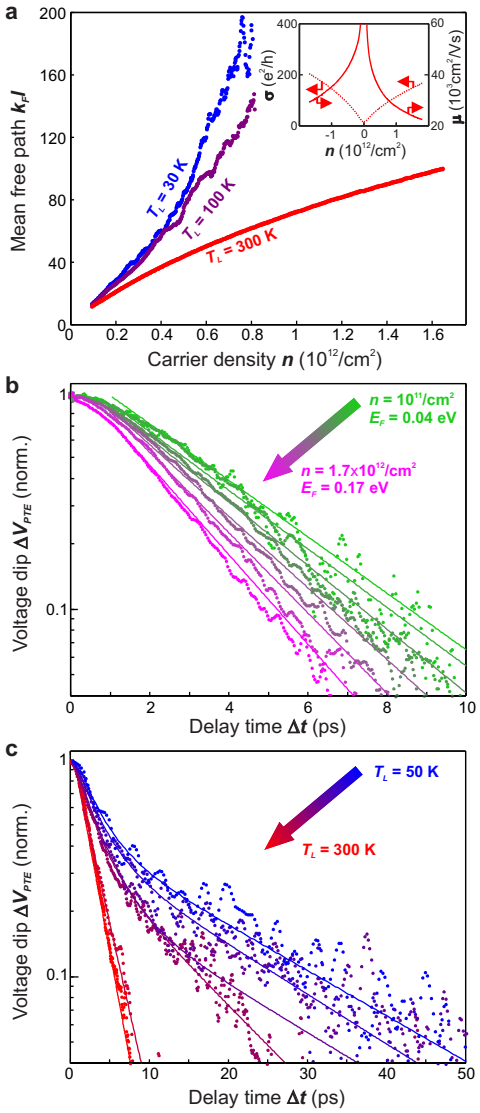

FIG. 2: **The effect of doping and lattice temperature. a)** From four-probe transport measurements, we extract the dimensionless mean free path parameter $k_{\rm F}\ell$ as a function of carrier density for three different lattice temperatures. These data show that carrier scattering in our hBN-encapsulated graphene is much less efficient than in SiO_2-supported graphene where $k_{\rm F}\ell$ is typically 10 or less, and where disorder-assisted supercollisions constitute the dominant cooling mechanism [26–28]. The inset shows the conductivity and mobility vs. gate-induced carrier density. By comparing four-probe and two-probe measurements we find that each contact has a contact resistance of 5 –8 kΩ. **b-c)** The dynamics of the photovoltage dip $\Delta V_{\rm PTE}$, showing that hot-carrier cooling becomes faster upon increasing the carrier density **(b)** and upon increasing the lattice temperature **(c)**. Panel **b** is measured at a lattice temperature of $T_L = 300$ K and panel **c** at a carrier density of $n \approx 1.7 \times 10^{12}/\text{cm}^2$. The solid lines are bi-exponential guides to the eye.

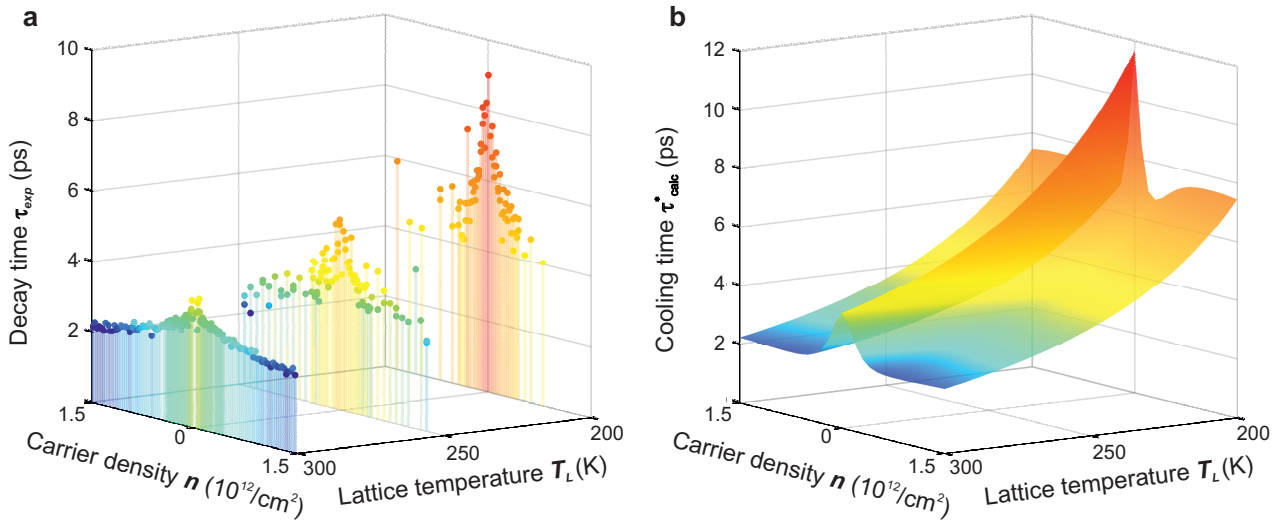

FIG. 3: **Qualitative comparison with hyperbolic hBN cooling.** Comparison between the experimental decay time τ_{exp} extracted from the dynamics of the photovoltage dip **(a)** and the predicted near-equilibrium cooling time τ^*_{calc} for super-Planckian cooling to hyperbolic hBN phonons **(b)**. Both in experiment and theory, we vary the carrier density and lattice temperature.

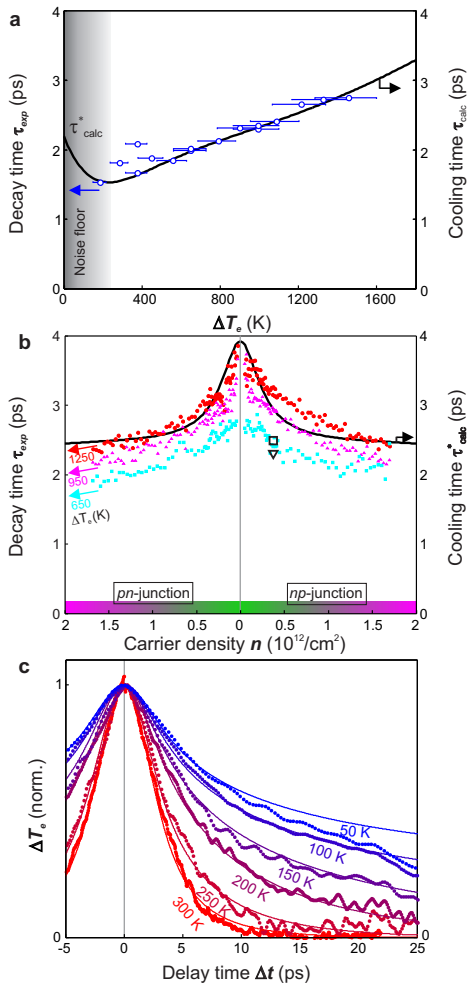

FIG. 4: **Quantitative comparison with hyperbolic hBN cooling.** **a)** Comparison between measured decay time $\tau_{\rm exp}$ (blue symbols and left vertical axis) and calculated cooling time $\tau_{\rm calc}$ (solid black line and right vertical axis) as a function of electron temperature *without any adjustable parameters*. **b)** The measured decay time $\tau_{\rm exp}$ (symbols and left vertical axis) at room temperature as a function of carrier density for three different laser powers, compared with the near-equilibrium cooling time $\tau^*_{\rm calc}$ (solid line and right vertical axis) according to super-Planckian cooling to hyperbolic hBN phonons *without any adjustable parameters*. The open square (triangle) shows the obtained decay time from time-resolved optical (terahertz) spectroscopy for $\Delta T_{\rm e} = 600 \pm 200$ K. **c)** Comparison of the complete cooling dynamics as measured (data points) and calculated (solid line) for $n = 0.06 \times 10^{12}/{\rm cm}^2$ for varying lattice temperature. The calculated dynamics are convoluted with a Gaussian function representing the experimental time resolution. We find an initial temperature increase of $\Delta T = 300$–500 K for all temperatures, except 1250 K for $T_{\rm L} = 300$ K. The lower ΔT is related to the larger effective photocurrent spot size.

Methods

Extraction of the initial hot carrier temperature — The measured photovoltage V_{PTE} scales with the *time-averaged* increase in electron temperature $\langle T_{\mathrm{e}} - T_{\mathrm{L}} \rangle$. In the case of cooling length smaller than the laser spot size (which is the case at room temperature) the relevant heat equation gives a simple linear scaling between peak and average increase in T_{e}, governed by the interfacial heat conductivity Γ. We assume that Γ and the Seebeck coefficient are constant with power [40], so that the photovoltage as a function of power directly represents the peak T_{e} increase as a function of power: $V_{\mathrm{PTE}} = a(T_{\mathrm{e}} - T_{\mathrm{L}})$. For undoped graphene, the peak T_{e} after illumination with laser power P is $T_{\mathrm{e}} = \sqrt[3]{T_{\mathrm{L}}^3 + bP}$, where b is a constant that depends on laser repetition rate f, absorption coefficient η_{abs}, heating efficiency η_{heat} and spot size L_{spot}. The cube root comes from the T^2-scaling of the electronic heat capacity for un-doped graphene (we apply this analysis to a low carrier density of $0.06 \times 10^{12}/\mathrm{cm}^2$). By fitting V_{PTE} as a function of P, we extract the constants a and b, which allows us to recover the power-dependent peak T_{e} (see Supp. Fig. 7). We verify the obtained constant b, and find good agreement when using an absorption of $\eta_{\mathrm{abs}} = 1\%$ (due to the layered dielectrics), a heating efficiency of $\eta_{\mathrm{heat}} = 80\%$ and a spot size of $L_{\mathrm{spot}} \sim 2\ \mu\mathrm{m}$.

Numerical calculations — Theoretical curves are obtained by numerically integrating Eq. (1) [31]. The non-local conductivity is connected to the density-density response function of graphene, $\chi_{nn}(k, \omega)$, by the formula $\sigma(\omega, k) = ie^2\omega\chi_{nn}(k, \omega)/q^2$. Within the random-phase approximation, we approximate $\chi_{nn}(k, \omega)$ with its non-interacting expression, which has been given in Refs. [41–44]. Neglecting retardation effects, the surface admittance is connected to the screened Coulomb interaction between two electrons in graphene, $V(k, \omega)$, by the formula $Y(\omega, k) = -ie^2\omega V^{-1}(k, \omega)/q^2$. The expression for $V(k, \omega)$ is given, for graphene embedded into slabs of hBN and in the presence of non-hyperbolic dielectrics and metallic gates, in Ref. [45].

Data availability statement

The data that support the plots within this paper and other findings of this study are available from the corresponding author upon reasonable request.